

# Wave-current interaction: Effect on the wave field in a semi-enclosed basin



A. Benetazzo <sup>\*</sup>, S. Carniel, M. Sclavo, A. Bergamasco

*Institute of Marine Sciences, National Research Council (ISMAR-CNR), Venice, Italy*

## ARTICLE INFO

### Article history:

Available online 7 January 2013

### Keywords:

Wave-Current Interaction  
Significant wave height  
COAWST  
Adriatic Sea  
Gulf of Venice

## ABSTRACT

The effect on waves of the Wave-Current Interaction (WCI) process in the semi-enclosed Gulf of Venice (northern region of the Adriatic Sea) was investigated using the Coupled Ocean–Atmosphere–Wave–Sediment Transport (COAWST) modeling system. COAWST relies on the ocean model ROMS (Regional Ocean Modeling System), the wave model SWAN (Simulating WAves Nearshore), and the CSTMS (Community Sediment Transport Modeling System) routines. The two-way data transfer between circulation and wave models was synchronous via MCT (Model Coupling Toolkit), with ROMS providing: current field, free surface elevation, and bathymetry to SWAN. For coupling, the 3-D current profiles were averaged using a formulation which integrated the near-surface velocity over a depth controlled by the spectral mean wavenumber. COAWST system was implemented on a parent grid (with horizontal resolution of 2.0 km) covering the whole Adriatic Sea with one-way nesting to a child grid resolving the northern area (Gulf of Venice) at a resolution of 0.5 km. The meteorological forcings provided by the operational meteorological model COSMO-I7 (a mesoscale model developed in the framework of the COSMO Consortium) were used to drive the modeling system in the period bracketing September 2010–August 2011. The adopted winds and the simulated waves were compared with observations at the CNR-ISMAR Acqua Alta oceanographic tower, located off the Venice littoral. Wave heights and sea surface winds were also compared with satellite-derived data. The analysis of WCI was performed on the child grid over the winter season (January–March 2011) with particular focus on the waves generated by prevailing and dominant winds blowing on the Adriatic Sea: Bora and Sirocco. Due to the variable wind direction with respect to the ocean current direction different effects on WCI were depicted, showing that within the northern Adriatic Sea the ocean–wave interactions are strongly dependent on the wind forcing direction. Further investigations reveal that, when applied to intense storms, the effect of coupling on waves results in variations of significant wave height up to 0.6 m, with some areas experiencing significant increase/decrease of wave spectral energy for opposite/following currents respectively.

© 2012 Elsevier Ltd. All rights reserved.

## 1. Introduction

Interaction between oceanic waves and current represents one of the primary driving forces in coastal and offshore areas. Sea gravity waves and surface circulation are mostly governed by the same driving factor (the atmospheric wind) and propagates in the same medium (the oceanic water). Waves and current form a complex system which is usually discussed assuming distinctly the influence of waves on hydrodynamics and the influence of wave on currents. This broad topic is usually referred to with the general term of Wave-Current Interaction (WCI) that, from the general point of view, traces back to the theoretical works of Longuet-Higgins (1970) on longshore currents flows produced by waves, and to the studies of the dynamics of waves in a moving medium (Tayfun et al., 1976).

Massel (1996) reviewed some formulations to predict the propagation of randomly distributed waves in an ambient current. These solutions, which are based on the kinematical equation for the density of waves and on the principle of wave action conservation, permit to estimate analytically the influence of a current on wave parameters (e.g., the local spectral energy density). In absence of wave breaking, the local wave amplitude is given by (Phillips, 1977)

$$\frac{A}{A_0} = \frac{c_0}{\sqrt{c(c + 2U)}} \quad (1)$$

where  $A$  is the wave amplitude and  $c$  is the wave phase speed in presence of an ambient current  $U$ , whereas the variables in a medium with null ambient current are marked by the subscript 0. The ratio  $A/A_0$  is illustrated as a function of wave period  $T$  and ambient current speed  $U$  in Fig. 1, which shows that waves propagating in a direction opposing the current (i.e.,  $U < 0$ ) are those most affected by the current.

\* Corresponding author. Address: CNR-ISMAR, Arsenale-Tesa 104, Castello 2737/F, I-30122 Venice, Italy. Tel.: +39 041 2407952; fax: +39 041 2407930.

E-mail address: [alvise.benetazzo@ismar.cnr.it](mailto:alvise.benetazzo@ismar.cnr.it) (A. Benetazzo).

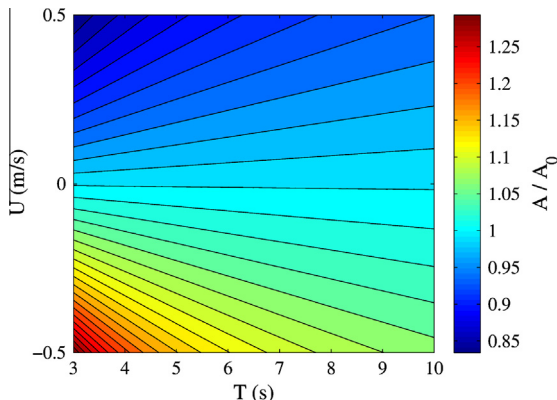


**Fig. 1.** Modification of wave amplitude  $A$  of surface waves with period  $T$  moving from still water to a region of current with velocity  $U$ , starting from still water. Positive values of  $U$  indicate a following current, whereas a negative  $U$  refers to wave trains subject to an opposite current.

Recently there have been quite a few theoretical works dealing with WCI, and in particular about oceanic flows forced by waves. Among others, McWilliams et al. (2004), Arduin et al. (2008), Mellor (2008) and Bennis et al. (2011) proposed several analytical solutions to estimate the main effects of propagating waves on the ocean current. In particular, Mellor (2008) proposed a radiation stress tensor which originated a pressure field demonstrated to be not consistent by Arduin et al. (2008). Then, Arduin et al. (2008) and Bennis et al. (2011) derived a consistent closure of the equations, and the validity of their work was demonstrated by Michaud et al. (2011).

At oceanic scales, wave models are based on balance of the spectral wave action balance equation (Gelci et al., 1957; Hasselmann, 1962; Komen et al., 1994; Mei, 1989), providing synthetic parameters of wave states. This allows operational wave forecasting systems to disseminate daily global or local wave conditions (Janssen, 2008). Generally, the integration of wave action equation is performed over a computational domain which does not account for the presence of currents. Successful applications under such hypothesis are numerous, and confining the discussion within the Adriatic Sea, examples can be found in Signell et al. (2005) and Dykes et al. (2009). However, wave action balance equation can account for an ambient current (Whitham, 1974) and numerical models are able to propagate the wave spectrum on a moving medium.

Benefiting from increase of numerical models efficiency and computational capabilities, recent applications of ocean-wave coupling have been considerably growing in the last decade. Osuna and Monbaliu (2004) studied the WCI in the southern North-Sea using a numerical coupling scheme allowing the data transfer between the WAve prediction Model WAM (Hasselmann, 1988) and a 2-D vertically integrated hydrodynamic model. With current speed up to 1 m/s, the authors found differences for significant wave heights and mean periods of about 0.2 m and 1 s, respectively. An experimental study of current effect on waves in a basin and its comparison with Simulating WAves Nearshore model (Booij et al., 1999) was proposed by Soares and de Pablo (2006) and Rusu and Soares (2011), who found a good agreement between the SWAN calculations of wave spectra and experimental results.

Warner et al. (2010) developed and applied to a hurricane scenario the same 3-D COAWST system used in this study, forced with the atmosphere Weather Research and Forecasting model (Skamarock et al., 2005). They showed that in certain conditions the significant wave height increases by as much as 20% when a wave system meets an opposite current. Similar results were obtained by Fan et al. (2009b) who found a reduction in the wave energy

when including an oceanic current following the waves. The authors also highlight that WCI improve hindcast and forecast of wave energy and, as a consequence, significant wave height. Another successful development of a coupled current-wave model is found in Bolanos et al. (2011), who implemented the circulation Proudman Oceanographic Laboratory Coastal-Ocean Modeling System (POLCOMS) and WAM models in the Northwestern Mediterranean Sea. Due to the low currents simulated, the authors found small differences between wave parameters (height and period) computed with WAM vs. those obtained by the same model once coupled with POLCOMS. Successful application of coupled POLCOMS-WAM in storm conditions is given in Brown et al. (2011). With the purpose of setting up an operational storm surge forecasting system in the Adriatic Sea, Roland et al. (2009) accounted for the influence of waves on water levels. Example of inclusion of ambient current in an operational ocean wave forecasting system is provided by the European Centre for Medium-Range Weather Forecasts (ECMWF), which found significant wave height modifications up to 0.5 m in presence of an ocean current (Hersbach and Bidlot, 2008).

Since all the cited studies showed the importance to account for ocean circulation when modeling waves in storm conditions, we aimed at investigating WCI in the Adriatic Sea, where wind wave storms are rather frequent (Benetazzo et al., 2012; Bignami et al., 2007; Cavalieri et al., 1989; Dykes et al., 2009). Adriatic Sea is an elongated (about 700 km long and 200 km wide) semi-enclosed basin delimited on three of its sides by the Italian coasts and the Balkans, and connected to the Mediterranean Sea by the Otranto Strait (Fig. 2). The Adriatic Sea extends mostly in the NW–SE direction, from the shallow Gulf of Venice to the Otranto strait. The so-called Gulf of Venice is located in the northern region of the Adriatic Sea, having dimensions of about  $200 \times 200 \text{ km}^2$ . This area is characterized by gentle slopes and relatively shallow depths, reaching maximum values up to 80 m in its southern region.

The most frequent winds blowing on the Adriatic Sea are the so-called Bora and Sirocco (Bignami et al., 2007), which cause high waves in the Adriatic Sea, although Bora waves are generally fetch-limited. In particular, Bora is a North–Eastern (Fig. 3), dry and cold wind, usually channeled through the Dinaric Alps and regarded as one of the Cold Air Outbreak (CAO). Bora is a gusty wind, particularly strong during the winter season over the northern and central Adriatic Sea (up to 15 m/s for several days, with gusts up to 50 m/s), which causes enhanced local cyclonic flow (Bergamasco and Gačić, 1996; Paklar et al., 2001). Contrary to Bora, the South–Eastern Sirocco waves are not fetch-limited and therefore characterized by a progressive growth; although Bora winds can attain

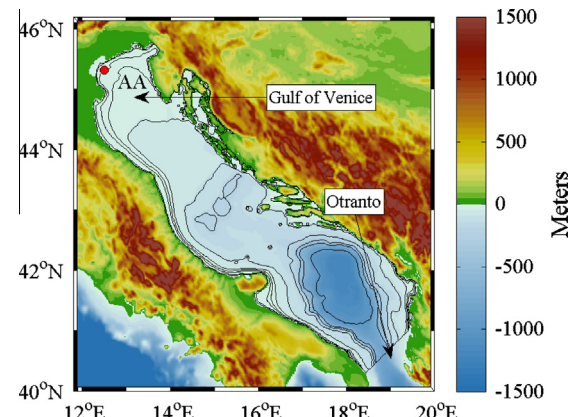


**Fig. 2.** Adriatic Sea bathymetry. The AA marker shows the Acqua Alta platform location.

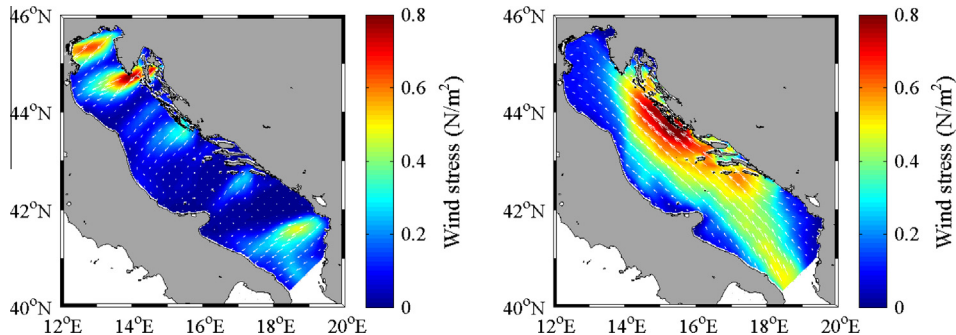


**Fig. 3.** Example of COSMO-I7 model output. Bora (left panel) and Sirocco (right panel) wind stress fields over the Adriatic Sea surface (10-m height) averaged over 2011 January, 27–29 and 2011 February, 15–17, respectively.

very high speed suddenly, Sirocco can grow slowly, reaching the highest speeds on the eastern Adriatic regions (Fig. 3), and generally it decreases while proceeding to the western coasts as pointed out by Signell et al. (2005).

The Adriatic hydrography and circulation have been studied since the end of the 18th century, and are thus described in many papers, among which we mention the review by Orlic et al. (1994) and the in situ analysis by Artegiani et al. (1997a, b) based on an extensive hydrographic data record ranging from 1911 to 1983 (Cushman-Roisin et al., 2001). We also refer to a volume (EU, 1999) on the northern Adriatic eutrophication issue, of which the physical component includes both in situ and modeling efforts (Bignami et al., 2007). More recently, this basin has been the site of a multi-project effort (Lee et al., 2005) investigating the influence of the wind and marine circulation on sediment distribution and deposition patterns. However, to our best knowledge, no examples of fully coupled wave-ocean 3-D model were implemented in the Adriatic region. With this paper we intend to fill this gap, specifically aiming at disentangling the effects of the wave on currents using a high resolution model in case of wind-driven circulations.

It is important to stress that it has been repeatedly proven critical to utilize high resolution wind forcing fields and circulation models, at least to model particular events in Adriatic marine circulation, if not its longer term (e.g., seasonal) characteristics. The use of low resolution winds in fact necessarily implies a calibration factor to better reproduce wind-driven circulation. This is particularly evident in the case of the cross-basin Bora pattern, because of the complexity and small scale of Adriatic orography is often poorly reproduced in atmospheric models. The Bora flow is seen to be composed of an alternation of high and low wind speed ‘strips’ crossing the Adriatic in correspondence of the fine scale (10–100 km) Balkanic orographic lows and highs. This causes a cyclone–anticyclone pattern in the circulation, with consequent upwind branches towards the eastern boundary, often unresolved when low resolution wind forcing is used (Bergamasco and Gačić, 1996; Paklar et al., 2001; Pullen et al., 2003; Signell et al., 2005).

Along this line of thought, we conducted some numerical experiments of WCI in the northern Adriatic Sea (Gulf of Venice) with the high-resolution COAWST system within the period bracketing September 2010–August 2011. In particular, we investigated the importance of including the effect of WCI to simulate waves using SWAN, implemented during the winter season ranging from January to March 2011. The COAWST system was set allowing a two-way coupling between SWAN and ROMS, with atmospheric forcings provided by the high-resolution model COSMO-I7. Within the simulated period, measurements of wave heights, current velocity, and wind speed were collected at Acqua Alta tower in the northern Adriatic Sea (Fig. 2). These observations, together

with satellite measurements, were used to evaluate the SWAN predictions in storm and non-storm conditions.

The outline of the paper is as follows. In the next Section, the governing equations of SWAN and ROMS numerical models are outlined together with details about the WCI and atmospheric model COSMO-I7 specification. In-situ and satellite-borne observations are presented in Section 3, with a comparison between modeled and measured data. In Section 4 we use the COAWST system to estimate the influence of current on waves. Finally, we provide a discussion and conclusion in Section 5.

## 2. Methods

The COAWST modeling system was here used in the Adriatic Sea to assess the influence of ocean circulation on surface waves. The simulations were based on a two-way coupling between ROMS and SWAN running on the same computational grid. The atmospheric forcing was uncoupled and fields were provided by the high-resolution COSMO-I7 model.

### 2.1. ROMS ocean model

The oceanic circulation was simulated using the COAWST system, based on Regional Ocean Modeling System (ROMS) version 3.4 (<http://www.myroms.org>). ROMS solves finite-difference approximations of the 3-D Reynolds-averaged equations for conservation of mass, momentum, and heat using a Generic Length Scale (GLS) turbulence approach (Kantha and Carniel, 2003; Umlauf and Burchard, 2003), with the implementation of Warner et al. (2005). Wind-driven circulation, mixing, and heating or cooling of surface waters were calculated using the Coupled Ocean–Atmosphere Response Experiment (COARE) 3.0 bulk flux algorithms with short wave radiation, wind, air temperature, humidity, and atmospheric pressure. A recursive Multidimensional Positive Definite Advection Transport Algorithm (MPDATA) advection is chosen to model the tracers dynamics (Smolarkiewicz, 1983, 1984).

### 2.2. SWAN spectral wave model

In the present work, the wind wave simulations were carried out using the Simulating WAves Nearshore (SWAN) model, version 40.81 (see Booij et al., 1999; and <http://www.swan.tudelft.nl>). SWAN is a state-of-the-art 3rd generation spectral wave model which computes random, short-crested wind-generated waves in offshore and coastal regions. The model describes the generation, evolution and dissipation of the wave action density spectrum  $N(\text{space}, \text{time}; \sigma, \theta)$ , where  $\theta$  is the wave propagation direction,

and  $\sigma$  is the wave relative frequency. SWAN solves a radiative time-dependent transport equation in the variable  $N$ , accounting for the wind input, the wave-wave interactions, and the dissipation terms both in deep and shallow waters. The ambient current affects the density spectrum balance in two ways. One way is that  $N$  will be propagated with a velocity modified by the local ocean current. A second way is that the effects of ocean currents are accounted for by using the apparent local wind speed and direction to modify the wind stress, for instance as analyzed by Kara et al. (2007). The wind speed modification by the local current is implemented in COAWST assuming the atmosphere flow relative to a moving frame: the wind speed is shifted by the ocean current velocity. This hypothesis allows guessing from COSMO-I7 10 m wind speed the effect of ocean current on surface stress. A commentary on the validity and limits of such a hypothesis is provided by Hersbach and Bidlot (2008).

The governing equation of  $N(\lambda, \varphi, t; \sigma, \theta)$  in spherical co-ordinates (i.e., the space is described by the two variables longitude  $\lambda$  and latitude  $\varphi$ ) reads,

$$\frac{\partial N}{\partial t} + \frac{\partial c_\lambda N}{\partial \lambda} + \frac{\partial c_\varphi N}{\partial \varphi} + \frac{\partial c_\sigma N}{\partial \sigma} + \frac{\partial c_\theta N}{\partial \theta} = \frac{S_{TOT}}{\sigma} \quad (2)$$

The first term represents the kinematics of the energy balance. The second term accounts for the wave energy propagation in the spherical space, with the flux convected by the propagation velocity of wave energy. In the geographical space, this velocity is given by

$$\begin{aligned} c_\lambda &= \frac{1}{R \cos \varphi} (c_g \cos \theta + u_\lambda) = \frac{1}{R \cos \varphi} \left( \frac{1}{2} \left( 1 + \frac{2kd}{\sinh(2kd)} \right) \frac{\sigma k}{k^2} \cos \theta + u_\lambda \right) \\ c_\varphi &= \frac{1}{R} (c_g \sin \theta + u_\varphi) = \frac{1}{R} \left( \frac{1}{2} \left( 1 + \frac{2kd}{\sinh(2kd)} \right) \frac{\sigma k}{k^2} \sin \theta + u_\varphi \right) \end{aligned} \quad (3)$$

where  $R$  is the radius of the Earth,  $c_g$  represents the magnitude of the group velocity vector  $\mathbf{c}_g = [c_g \cos \theta, c_g \sin \theta]$  which is function of the wavenumber vector magnitude  $k = |\mathbf{k}|$  and the water depth  $d$ . In Eq. (3), and  $u_\lambda$  and  $u_\varphi$  are the two components of the ambient current in longitude and latitude direction, respectively. The third term of Eq. (2) denotes the flux of energy in  $\sigma$ -space and the radian frequency variations due to depth and ambient current. The propagation velocity in the spectral  $\sigma$ -space is given by

$$c_\sigma = \frac{\partial \sigma}{\partial t} \left( \frac{\partial d}{\partial t} + \mathbf{U} \cdot \nabla d \right) - c_g \mathbf{k} \cdot \frac{\partial \mathbf{U}}{\partial s} \quad (4)$$

where  $s$  is the space coordinate in the wave propagation  $\theta$ , and  $\mathbf{U} = [u_\lambda, u_\varphi]$  is the ambient current vector. The last term of the left-hand side of Eq. (2) accounts for the wave refraction due depth- and current-induced. The propagation velocity in the  $\theta$ -space reads

$$c_\theta = -\frac{1}{k} \left( \frac{\partial \sigma}{\partial d} \frac{\partial d}{\partial m} + \mathbf{k} \cdot \frac{\partial \mathbf{U}}{\partial m} \right) \quad (5)$$

with  $m$  corresponding to the space coordinate perpendicular to the wave propagation  $\theta$ . The effect of currents on wave energy is explicitly introduced in the propagation terms reported in Eqs. (3)–(5). On the right-hand side of Eq. (2),  $S_{TOT}$  variable describes the terms of energy source and sink, and the conservative redistribution of energy among wave spectral components. The dissipation term accounts for whitecapping, bottom friction, and depth-induced breaking; the nonlinear wave-wave interactions are described by the four-wave and three-wave interactions in deep-intermediate and shallow waters, respectively.

### 2.3. COSMO-I7 atmosphere model

To properly simulate winds in the semi-enclosed Adriatic Sea, high-resolution atmospheric models are necessary to adequately address the effect of the surrounding orography (Signell et al., 2005). They have also shown how the meteorological model resolution is crucial for reproducing accurately dominant and transient winds in the Adriatic region, suggesting, among other characteristics, that numerical tools with horizontal grid size smaller than 20 km can significantly improve the accuracy of meteorological forcing for wave numerical models.

In accordance to this, in this study the atmospheric forcings employed (i.e., 10-m height wind field, atmospheric pressure, air temperature, air humidity, cloud cover, rain intensity, shortwave solar radiation) were provided by the Italian operational atmospheric model COSMO-I7, a local implementation of the Lokal Model (Steppele et al., 2003). COSMO-I7 is the Italian version of the COSMO Model, a mesoscale model developed in the framework of the COSMO Consortium (<http://www.cosmo-model.org>). It is a non-hydrostatic, 3-D numerical weather prediction model with a 7 km horizontal resolution, 35 vertical terrain-following levels, providing outputs every 1 h. Initial and lateral boundary fields for COSMO-I7 are provided by the global model Integrated Forecast System (IFS) from the European Centre for Medium-Range Weather Forecasts (ECMWF). COSMO-I7 covers the domain 2–22°E and 32–52°N, which has an extension of 2000 × 1500 km<sup>2</sup>. COSMO-I7 runs operationally for 00:00 UTC at the Emilia Romagna Region Meteorological and Hydrological Service (ARPA-EMR-SIMC, <http://www.arpa.emr.it/sim/pagine/home/index>) and provides 72-h forecasts. The meteorological forcing fields for COAWST were obtained from the daily COSMO-I7 runs accounting for the first 24-h forecast, and they were linearly interpolated in space to the ROMS and SWAN model grids.

### 2.4. COAWST system set-up

COAWST system was implemented in the Adriatic Sea for a 12-month hindcast period, ranging from 2010 September, 1 to 2011 August, 31, and it was based on two different curvilinear orthogonal computational grids. The coarse parent grid (with horizontal spacing of 2.0 km in both directions, and 20 vertical sigma-levels) covers the whole Adriatic Sea, and it is the same adopted in other previous studies (Bignami et al., 2007; Boldrin et al., 2009; Carniel et al., 2009), locating the southern open boundary at the Otranto Strait (Fig. 2). Here, ROMS open boundary conditions (sea surface elevation, vertical distribution of 2-D momentum, temperature and salinity) were taken from the Mediterranean Forecasting System (Pinardi et al., 2003) running at INGV (Istituto Nazionale di Geofisica e Vulcanologia), released through MyOcean service (<http://www.myocean.eu.org/>). Besides, along the boundary five tidal constituents were imposed (namely, M2, S2, N2, O1, K1), as obtained through the Oregon State University (OSU) model (<http://volkov.oce.orst.edu/tides/>). For 3-D passive tracers and baroclinic fields the radiative boundary condition (Orlanski, 1976) was prescribed. For the ocean model initial conditions (at 00:00 UTC on the 1st September 2010) of 3-D velocity, depth-integrated 2-D velocity, free-surface level, temperature and salinity were obtained from operational version running at the University of Ancona (Russo et al., 2012). The sediment model was initialized with zero sediment concentration in the whole computational domain. Daily-averaged time series of fresh water and sediment concentration supplies from the Po river were imposed (Bever et al., 2009; Harris et al., 2008). In order to better account for the impact on coastal circulation and sediment supply, the flow of other rivers based on monthly-mean values using climatological estimates (Raicich, 1994) were also imposed, for a total of 26 rivers. The ROMS coarse

grid ran with a 60 s baroclinic time-step, with 20 barotropic time-steps between each baroclinic time-step. Model outputs (e.g., 3-D and 2-D velocity components, free-surface, temperature and salinity fields) were saved every 0.5 h. The sediment model time step was chosen equal to the time step used to run the ocean model, and the outputs saved were: suspended concentration, bed layer fraction, bed load, and sediment layer thickness.

The adopted child grid has horizontal spacing of 0.5 km, and it was offline nested (Mason et al., 2010) to the parent grid in the northern Adriatic Sea sub-region (Fig. 4 and 5). At the southern boundary of the fine grid, free surface, 2-D momentum, 3-D momentum, salinity, temperature, and sediments fields from the parent model were imposed with a 0.5-h time-step. A Chapman condition (Chapman, 1985) was imposed to the free-surface and a Flather condition (Flather, 1976) used to specify the 2-D momentum. The 0.5-km resolution was here used since the internal Rossby radii of deformation and the vertical dynamical modes in the northern Adriatic Sea range between 10 km in summer and 1 km in winter (Bergamasco et al., 1996). The consequence is that a 2-km grid is not always an eddy resolving grid, and the downscaling to 0.5 km is necessary to capture almost completely the internal dynamics of ocean circulation. On the child grid, the baroclinic and barotropic time-steps used in ROMS were the same adopted for the parent grid. In this specific model setting, the output were saved every 3 h.

SWAN was implemented on the parent and child grids by discretizing the wave action density with 24 equally spaced directions and 32 intrinsic frequencies  $f$  geometrically distributed, such that  $f_{n+1} = 1.1f_n$ , with  $f_1 = 0.05$  Hz. SWAN was run in third generation mode and the quadruplet wave-wave interactions in deep water were carried out with the Discrete Interaction Approximation (Hasselmann et al., 1985). Exponential wave growth by wind and whitecapping were evaluated with the expressions due to Komen et al. (1984) with default coefficients (SWAN, 2012). The energy dissipation due to depth-induced wave breaking (Battjes and Janssen, 1978) and to bottom friction (Madsen et al., 1988) was also activated using default settings. A first order, Backward Space, Backward Time (BSBT) scheme was used to discretize the wave action fluxes in geographical space, while in the spectral space a hybrid central/upwind scheme was chosen (SWAN, 2012). SWAN was run in non-stationary mode (i.e., the wave action density spectrum  $N$  evolved in time), with a 600 s time step, and the outputs saved

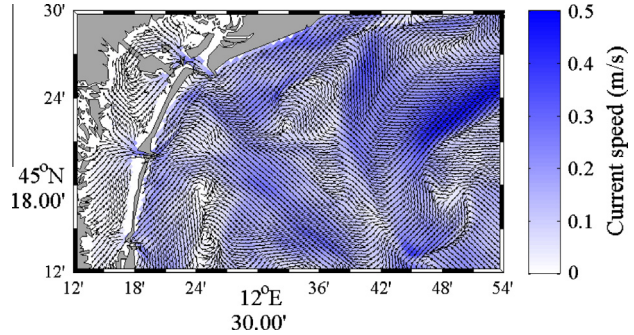


**Fig. 5.** Example of current speed computed by COAWST modeling system in the Gulf of Venice. For graphical purposes, current vector arrows are scaled to unity length.

every 0.5 and 3 h for the coarse and fine grids, respectively. On the parent grid, SWAN was configured assuming that no waves entered the area and that waves were able to leave the area freely at the southern boundary. The computation on the coarse grid provided the shape of the spectra at the boundary of the fine grid, imposed with a 30-min time step. For SWAN, initial conditions were obtained by running the model for stationary conditions. Wave parameters related with the energy spectra and computed for each computational cell were significant wave height ( $H_s$ ), second-moment wave period ( $T_{m02}$ ), and mean wave direction ( $\theta$ ).

In the configuration adopted for this study, the ocean model provides the wave model with currents, free surface elevation, and the bathymetry evolution, being the morphology module implemented in the ROMS model. There exist different possible approaches to define the current velocity field calculated by the circulation model which is then passed to the wave model. As waves mostly feel the surface velocity, one option is to send the velocity at first vertical level from the ocean to the wave model for coupling. Alternatively, the depth-integrated speed can be used, or the ocean current at the depth which modifies the apparent phase speed of the wave train (Fan et al., 2009a). Here, the horizontal current velocity field provided by the circulation model ROMS was transformed using the formulation proposed by Stewart and Joy (1974), and extended to finite depths by Kirby and Chen (1989). The proposed formulations account for the observation that short waves feel the current nearby the surface whereas longer waves are altered by currents extending from the surface to larger water depths. Consequently, ambient current velocity  $\mathbf{U}$  is function of the wavenumber  $k$ , i.e.,  $\mathbf{U}_k = \mathbf{U}(k) = [u_\lambda(k), u_\phi(k)]$ , and can be written as

$$\mathbf{U}_k = \frac{2kd}{\sinh(2kd)} \int_{-d}^0 \mathbf{U}(z) \cosh[2k(d+z)] dz \quad (6)$$

where  $\mathbf{U}(z) = [u_\lambda(z), u_\phi(z)]$  is the vertically non uniform current velocity profile calculated by ROMS. In COAWST system, the weighted average expressed by Eq. (6) was calculated with respect to the mean spectral wavenumber, and used by SWAN in Eq. (2). A discussion about the use of using Kirby and Chen (1989) formulation in numerical models is presented in Olabarrieta et al. (2012).

The fully coupled COAWST system also accounts for the effect of oscillating waves on the oceanic flows. To this end, the wave model provides to the ocean model: wave energy dissipation ( $\varepsilon_{br}$ ), significant wave height ( $H_s$ ), percent of breaking waves ( $Q$ ), surface peak wave period ( $T_p$ ), bottom mean wave period ( $T_{m,bot}$ ), mean wave direction ( $\theta_m$ ), average wave number ( $k$ ), wave orbital velocity near the bottom ( $U_{bot}$ ). In the adopted configuration of ROMS model, these wave parameters were used to predict surface

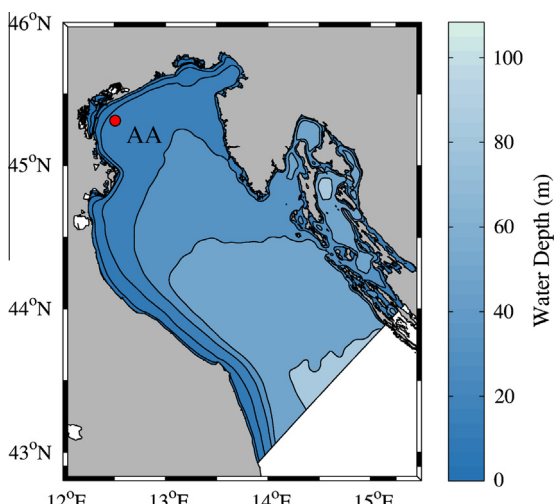


**Fig. 4.** Map of the Adriatic Sea bathymetry used by the COAWST modeling system in the Gulf of Venice (Northern Adriatic Sea). The AA marker shows the Acqua Alta platform location.

layer dynamics and roughness, bottom boundary layer closure, and momentum fluxes induced by waves (Olabarrieta et al., 2012; Warner et al., 2008). On the water surface, breaking waves produce an injection of kinetic energy: in these conditions, the near-surface mixing is stronger and the current velocity vertical gradient is reduced (Carniel et al., 2009 and references therein). In COAWST system, for breaking waves, the surface roughness length was parameterized as proportional to the significant wave height with a coefficient chosen equal to 0.5 (Stacey, 1999). In the COARE algorithm, the default option (Charnock, 1955) for wave roughness formulation in bulk fluxes was used. The stresses on the Bottom Boundary Layer (BBL) are parameterized with a formulation which represents the interactions of currents and wave motions over a movable bed. In the configuration adopted in the study, the wave-current BBL model described in Warner et al. (2008) is used.

The oceanic wave driven-flows and the effect of surface waves on mass flux transport were modeled with a Vortex-Force (VF) formalism (Kumar et al., 2012; McWilliams et al., 2004; Olabarrieta et al., 2012; Olabarrieta et al., 2011; Uchiyama et al., 2010). Following Kumar et al. (2012), in VF equations, wave averaging is considered in an Eulerian reference frame, and wave effects on ocean circulation enter in ROMS primitive equations as momentum and tracers fluxes. Horizontal and vertical hydrodynamic contributions are separated in conservative (VF terms) and non-conservative wave forces, including an adjustment of the pressure field with satisfies the presence of waves. The horizontal VF term can be written as:

$$\nabla \mathbf{F}_{hor} = -\hat{\mathbf{z}} \times \mathbf{u}_{st} (\hat{\mathbf{z}} \cdot \nabla_{\perp} \times \mathbf{u} + f) - w_{st} \frac{\partial \mathbf{u}}{\partial z} \quad (7)$$

where  $\mathbf{u}_{st}$  is the horizontal vector of Stokes velocity, and  $w_{st}$  is its vertical components;  $z$  is the vertical direction, with unit vector equal to  $\hat{\mathbf{z}}$ ;  $\mathbf{u}$  is the horizontal Eulerian mean velocity;  $f$  is the Coriolis parameters;  $\nabla_{\perp}$  represents the horizontal differential operator. The horizontal VF term includes an interaction between the vorticity of the Eulerian field and the Stokes drift, the Stokes–Coriolis force, and a convective acceleration. Non-conservative wave forces induce flow acceleration and dissipation. Accelerations are proportional to the wave energy  $\varepsilon_{br}$  dissipated in the breaking process (depth-induced and whitecapping) and are introduced as a body force (Kumar et al., 2011):

$$\mathbf{F}_w = \frac{\varepsilon_{br}}{\rho_0 \sigma} \cosh \left[ \frac{2}{\sqrt{2}} \frac{2\pi}{H_s} (z + d) \right] \mathbf{k} \quad (8)$$

where  $\rho_0$  is the reference water density. Wave-induced dissipations are the resulting effect on the apparent bed roughness due to the wave motion in the bottom boundary layer (Madsen, 1994). The pressure field correction  $P_{cor}$  is proportional to the square of  $H_s$ , and it is defined as:

$$P_{cor} = \frac{\sigma H_s^2}{32k \sinh^2(kd_{tot})} \int_{-d}^z \frac{\partial^2 \mathbf{k} \cdot \mathbf{u}}{\partial z^2} \sinh[2k(z - z')] dz' \quad (9)$$

$P_{cor}$  induces additional forces equal to  $-\nabla_{\perp} P_{cor}$  and  $-\frac{\partial P_{cor}}{\partial z}$  in the horizontal plane and vertical direction, respectively. The vertical VF term is expressed as:

$$\nabla \mathbf{F}_{vert} = -\mathbf{u}_{st} \cdot \frac{\partial \mathbf{u}}{\partial z} \quad (10)$$

In COAWST, Stokes drift are computed using bulk wave parameters such as the significant wave height, the mean wave number, and the mean direction of propagation. The 3-D Stokes velocities profile can be written as:

$$\begin{aligned} \mathbf{u}_{st}(z) &= \frac{\mathbf{k}}{c} \frac{\cosh[2k(d+z)]}{\sinh(2kd_{tot})} \frac{1}{8} g H_s^2 \\ w_{st}(z) &= -\nabla_{\perp} \cdot \int_{-d}^z \mathbf{u}_{st}(z) dz' \end{aligned} \quad (11)$$

where  $c$  is the wave phase speed. The use of integrated wave parameters to diagnose  $\mathbf{u}_{st}$  and  $w_{st}$  could lead to Stokes velocities less accurate (Tamura et al., 2012) than those estimated directly from wave spectra.

Throughout this study, the two-way coupled system (referred as 2WC) that included the transfer of terms described in this section was used in both parent and child grids. The two-way coupling between ROMS and SWAN was done synchronously with a 0.5-h time interval between coupling of models. To assess the influence of coupling, on the fine grid the uncoupled COAWST system (referred as UNC) was also run for the winter season from January to March 2011.

### 3. Evaluation of numerical model performances

For the whole hindcast period on the coarse grid (September 2010–August 2011), wind, waves, and currents were recorded at the ISMAR-CNR Acqua Alta tower, located in the northern Adriatic Sea (Lat = 45°18'83"N, Lon = 12°30'53"E, see Fig. 6), where local water depth is approximately 16 m. The waves and current were measured using a Nortek AS AWAC current profiler and wave directional system with a sampling rate of 2 Hz. AWAC instruments exhibits accuracies of 1 cm and 2° in wave elevation and direction, respectively. The accuracy for current is 1% of measured value. AWAC was programmed to collect twenty minutes of waveburst data every 30 min. Spurious data, common in Acoustic Doppler velocimeters, were despiked by using the method described in Goring and Nikora (2002). The wind speed was measured at a height of 15 m above mean sea level with a VT0705B SIAP anemometer, and recorded every 5 min. The observed wind speed was corrected to the standard 10-m reference level ( $U_{10}$ ), assuming winds taken in near-neutral conditions (Large and Pond, 1981; Massel, 1996).

In addition to Acqua Alta data, to analyze model predictions Jason-1 (NASA/CNES), Jason-2 (NASA/CNES/EUMETSAT/NOAA), and Envisat (ESA) remotely sensed significant wave height  $H_s$  and  $U_{10}$  were also considered (Fig. 6). Satellite-borne altimeter measurements, which are available at sparse time and are intrinsically spatially distributed permitted to evaluate the wave model accuracy

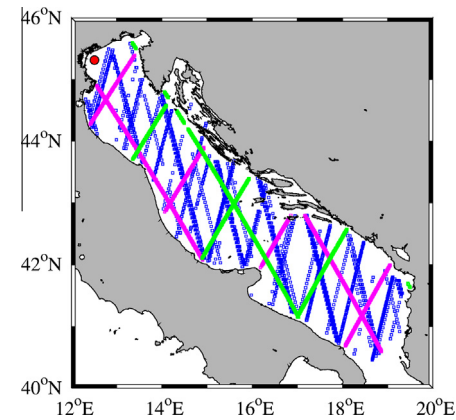


**Fig. 6.** Jason-1 (magenta), Jason-2 (green), and Envisat (blue) satellite tracks over the Adriatic Sea from 2010 September, 01 00:00 UTC to 2011 August, 31 23:30 UTC. The red marker shows the Acqua Alta platform location. (For interpretation of the references to colour in this figure legend, the reader is referred to the web version of this article.)

over a large area. This is significantly more important in an area like the Adriatic Sea, where the complex topography produces rapidly varying and spatially distributed sea surface wind fields (Dykes et al., 2009). A validation of the significant wave height  $H_s$  from both the Jason-1 and Envisat altimeters was done by Durrant et al. (2009), who found a Root-Mean-Square Difference between altimeters and buoy data of approximately 0.2 m. Johnsen et al. (2005) compared Jason-1 and ENVISAT altimeter wind speeds using buoy data, reporting mean value and standard deviation of differences of about 1 and 1.5 m/s, respectively. Similar values were found by Cavalieri and Sclavo (2006) in their comparison of ERS-1 altimeter wind speeds to buoy data in the Mediterranean and Adriatic Seas.

To allow a direct comparison with available model outputs, observations at *Acqua Alta* were interpolated onto COAWST and COSMO-I7 time base, while modeled data were extracted in the computational grid position nearest to the expected *Acqua Alta* tower location. In order to assess COSMO-I7 performances on the whole Adriatic Sea, modeled  $U_{10}$  were selected along a swath of 3.5 km and with a 0.5 h temporal proximity criterion with altimeter winds. A similar procedure was applied to COAWST outputs as far as wave parameters and ocean current vertical profiles are concerned. For modeled waves and currents, the spatial proximity criterion was limited to 1.0 km.

To evaluate the numerical model performances, the statistics used to compare modeled and observed data are *Bias*, Root-Mean-Square Difference (*RMSD*), linear correlation coefficient (*CC*), standard deviation of the fields (Taylor, 2001). Further indicators of the average performance of a model are given by the slope  $p$  of the best fit-line between model and observed data, and by the amplitude response error defined as  $E = 100(1 - p)$ .

Within the 12-month long simulated period, Fig. 7 illustrates a 3-month time series comparison of modeled and observed  $U_{10}$  at *Acqua Alta*. Within the period shown, all the peaks correspond to Bora events, except one Sirocco wind condition. The COSMO-I7 model captures the timing of the wind events, and there is no clear evidence of a magnitude reduction, differently to what observed by Signell et al. (2005) for four wind models (ECMWF, LAMBO, LAMI, COAMPS) operating in the Adriatic Sea area. Indeed, within the period shown in Fig. 7, Bora and Sirocco events that occurred with peak speeds greater than 10 m/s were well predicted. The same behavior is shown by the  $H_s$  and  $T_{m02}$  time series (Fig. 8 and Fig. 9), but with a smoother field.

The scatter diagram for wind speed at the *Acqua Alta* tower is shown in the left panel of Fig. 10, where the dashed tick line shows the linear best fit between modeled (COSMO-I7) and observed data. The wind speed average underestimation is characterized

by a response error  $E$  equal to 10% (Table 1), which reflects a good average performance of COSMO-I7 model. As expected (see Signell et al., 2005), COSMO-I7 model shows a rather large scatter for winds (*RMSD* = 2.12 m/s), which reduces the *CC* value to be equal to 0.77. At *Acqua Alta*, a 0.18 m/s (negative) bias in the modeled  $U_{10}$  data was found. In general, low wind speeds (below 5 m/s) were overestimated (bias is equal to 0.16 m/s) with a tendency towards underestimation as the wind speeds increase (above 10 m/s the bias becomes  $-1.43$  m/s). This underestimation of higher winds is typical in the Northern Adriatic Sea (Signell et al., 2005) especially during Bora episodes, when an airflow response reduction is operated by the mountain smoothing within the atmosphere numerical models (Cavalieri and Bertotti, 2003).

The ratio of standards deviations of model and observed data ( $R_{std}$ ) is equal to 1.03, therefore the two signals have approximately the same amplitude of the variation around the mean. The comparison between modeled and remotely sensed wind data shows a similar statistics (Table 1), with the slope of the best fit line equal to 0.98 (see right panel of Fig. 10). Note the overestimation by the altimeter for wind speeds below 5 m/s (bias = 0.82 m/s), and a negative bias ( $-0.52$  m/s) for high winds (above 10 m/s) corresponding to underforecasting the observed values on the average.

The SWAN model response error,  $E$ , is increased with respect to the meteorological model (Fig. 11 and Table 1). This is a consequence of the nature of waves that are an integrated effect of the space-time varying wind field. Assuming, for instance, the Pierson–Moskowitz spectral formulation (Pierson and Moskowitz, 1964), the  $H_s$  of a given sea states is proportional to the square of wind speed. The obvious implication is that an underestimation of the wind speed of, e.g., 10% causes the waves derived to be underestimated by a larger degree, up to 20%. Despite this effect, the overall evaluation of the wave model is satisfying and shows an improvement of the wave fields with respect to those analyzed in the same area by Signell et al. (2005), suggesting that atmosphere models have improved significantly over 5 years. In fact, the response error  $E$  for both  $H_s$  and  $T_{m02}$  (Fig. 11, Fig. 12, and Table 1) are in the order of 10%. COAWST wave outputs show little biases relative to *Acqua Alta* data:  $-0.01$  m for  $H_s$ , and  $-0.14$  s for  $T_{m02}$ . Along the same tendency, a bias for  $H_s$  of  $-0.02$  m shows a small systematic underestimation of modeled data relative to altimeters observations. Examining the scatter plots for waves, we observed an average positive deviation from observed small waves ( $H_s < 0.7$  m) at *Acqua Alta* (bias = 0.03 m) and remotely sensed (bias = 0.04 m). The underestimation in COAWST starts at around  $H_s = 1.2$  m and  $T_{m02} = 2$  s, and tends to increase for high waves ( $H_s$  and  $T_{m02}$  above 2 and 5 s, respectively), being the bias equal to  $-0.42$  m and  $-0.76$  s at *Acqua Alta*, and  $-0.16$  m for altim-

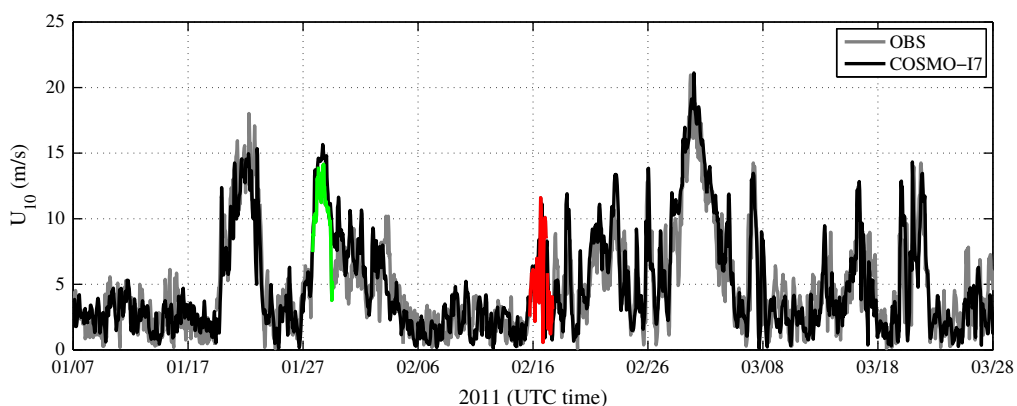


**Fig. 7.** Time series comparison of modeled (COSMO-I7) and observed (OBS) wind speed  $U_{10}$  at the oceanographic tower *Acqua Alta*. Example of Bora (green line) and Sirocco (red line) wind events are highlighted.(For interpretation of the references to colour in this figure legend, the reader is referred to the web version of this article.)

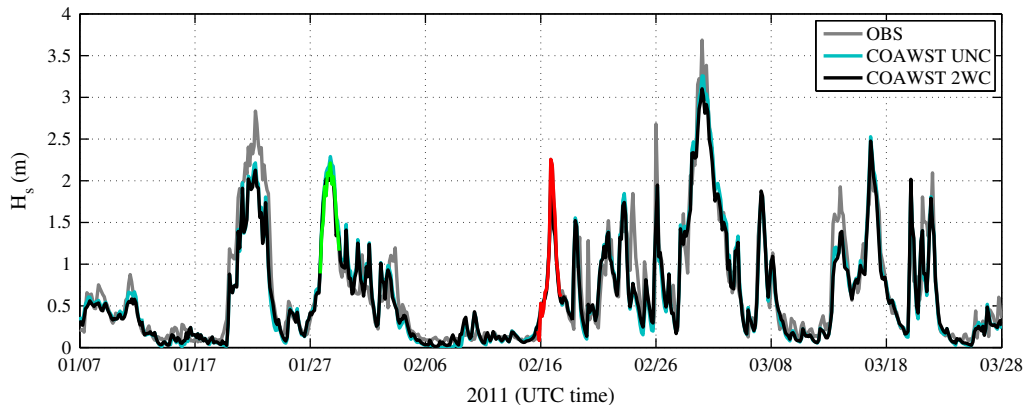


**Fig. 8.** Time series comparison of modeled (COAWST) and observed (OBS) significant wave height  $H_s$  at the oceanographic tower *Acqua Alta*. Simulated  $H_s$  are shown as computed by the fully coupled (2WC) and uncoupled (UNC) systems. Example of Bora (green line) and Sirocco (red line) wave events are highlighted.(For interpretation of the references to colour in this figure legend, the reader is referred to the web version of this article.)

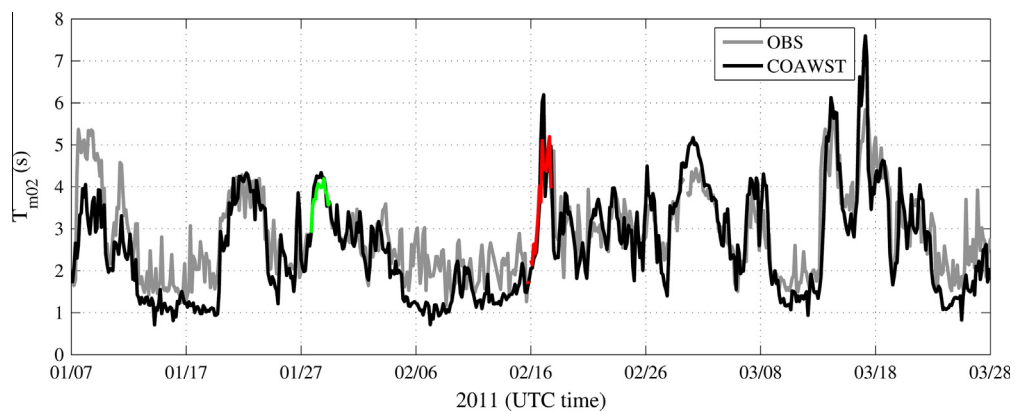


**Fig. 9.** Time series comparison of modeled (COAWST) and observed (OBS) mean period  $T_{m02}$  at the oceanographic tower *Acqua Alta*. Example of Bora (green line) and Sirocco (red line) wave events are highlighted.(For interpretation of the references to colour in this figure legend, the reader is referred to the web version of this article.)

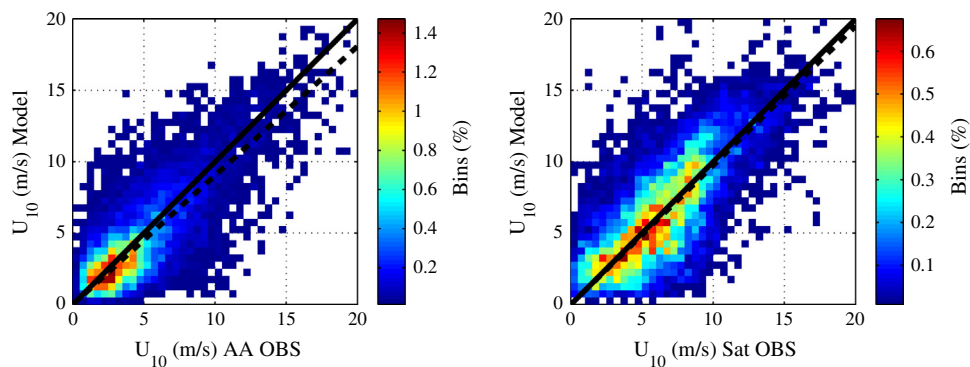


**Fig. 10.** Scatter diagrams of wind speed magnitude: numerical model/observations at *Acqua Alta* (left) and remotely sensed for the three satellite data merged on the whole Adriatic Sea (right). Scatter plot was created by binning the data into 0.50 m/s bins. The dashed black line is the linear regression while the black line represents the perfect fit between the two data sets.

**Table 1**  
Validation statistics for modeled  $U_{10}$ ,  $H_s$ , and  $T_{m02}$  comparisons with observations at *Acqua Alta* (AA) and remotely sensed (Sat).

Variable	$p$	Bias	RMSD	CC	$R_{std}$
$U_{10}$ -AA	0.90	-0.18 m/s	2.12 m/s	0.77	1.03
$U_{10}$ -Sat	0.98	0.07 m/s	1.82 m/s	0.72	1.11
$H_s$ -AA	0.89	-0.01 m	0.20 m	0.90	0.92
$H_s$ -Sat	0.94	-0.02 m	0.26 m	0.81	1.12
$T_{m02}$ -AA	0.92	-0.14 s	0.52 s	0.80	1.06

eter data. In general, wave data appear to be less scattered than wind data, and consequently significant wave height correlations are higher than wind correlations.

Finally, the effect of model downscaling on wave parameters is evaluated at *Acqua Alta* comparing model results of coarse and fine grid implementations. The effect of change in wave model resolution was originally investigated by Cavalieri et al. (1996) and recently by Osuna and Monbaliu (2004) who found small differences in wave parameters using WAM model on computa-

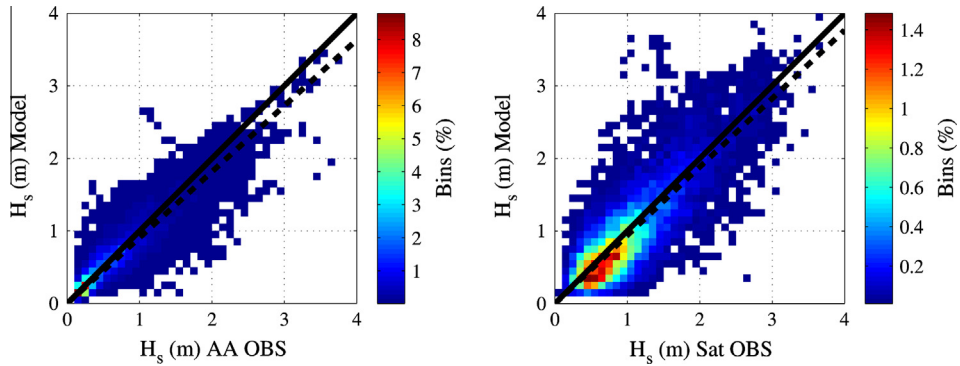


**Fig. 11.** Scatter diagrams of significant wave height: numerical model/observations at *Acqua Alta* (left) and remotely sensed for the three satellite data merged (right). Scatter plot was created by binning the data into 0.10 m bins. The dashed black line is the linear regression while the black line represents the perfect fit between the two data sets.

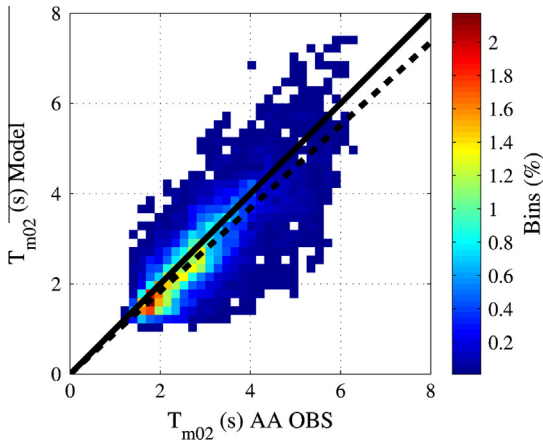


**Fig. 12.** Scatter diagram of wave period: numerical model/observations at *Acqua Alta*. Scatter plot was created by binning the data into 0.19 s bins. The dashed black line is the linear regression while the black line represents the perfect fit between the two data sets.

tional grids with resolutions of 1.0 and 3.0 km. In our implementations, the  $H_s$  values computed by the 0.5 km resolution model are in good agreement with those obtained using the coarser grid (2.0 km resolution), being the response error equal to 1%, the RMSD equal to 0.04 m, and CC = 1.00. The Bias is approximately null ( $-0.01$  m), indicating that the values computed by the fine grid were not systematically different from those of the coarse grid. Similar conclusions can be drawn analyzing the second moment wave period  $T_{m02}$ , being  $E = 2\%$ , Bias =  $-0.05$  s, RMSD = 0.17 s, and CC = 1.0.

#### 4. Current effect on the wave field

To investigate the effect of sea currents on waves, COAWST system was run on the Gulf of Venice fine grid for a three-month period covering the winter season from January 2011 to the end of March 2011. Within the simulated period, it was possible to focus on the wave storms with maximum  $H_s$  greater than 2.5 m in the northern Adriatic Sea (Fig. 8), as a result of wind speeds above 10–15 m/s (Fig. 7). From the run outputs two different stormy conditions were identified and isolated (see Fig. 7 and Fig. 8), representing situations of northeastern (Bora) and southeastern (Sirocco) winds. On January 27–29th, 2011, an intense Bora event occurred in the northern Adriatic Sea, generating measured wind speeds up to 14 m/s at the *Acqua Alta* tower.

This storm occurred during a time of neap tides when the observed semi-diurnal tidal range was closer to 0.6 m. On the other hand, on February 15–17th, 2011, a Sirocco wind blew in the Adriatic Sea with peaks up to 12 m/s. A spring tidal condition was observed with a tidal range of 1.4 m. For both storms, Fig. 13 shows the comparison of wind speed measured at *Acqua Alta* tower and modeled by COSMO-I7 model in the computational cell nearest to the tower geographical location. For comparison, the observed and modeled currents were computed using Kirby and Chen (1989) formulation (Olabarrieta et al., 2012).

During Bora conditions, wind channeling across the Istria peninsula produces main current streams moving from North–East to South–West (Book et al., 2007). Two subgyres are generated by this intense wind event (Fig. 14, left panel). One followed the northern Italian coast and recirculates in the proximity of the Po river delta, whilst the second, induced by the Kvarner Bora winds, approached the Italian coast and continues southward. Locally, average current speed reached 0.45 m/s, a value in accordance with ADCP historical observations in the same area during winter conditions (Book et al., 2005). Bora waves were oriented southwesterly (Fig. 14, right panel), apart from a small rotation to North in front of the Istria peninsula. In accordance to the wave action balance,  $H_s$  values were modified by the ocean current, experiencing a decrease/increase of energy (shoaling) when the waves propagated in a following/opposite ambient current (Fig. 15, left panel). During the storm, mean differences of  $H_s$  between the 2WC and UNC model runs reached 0.2 m. Comparing model wave heights to measurements at *Acqua Alta*, the over prediction in the significant wave height for UNC model (Fig. 16, left panel) may be accounted for by the overestimation in the wind speed (Fig. 13, left panel). The wave hindcast was slightly improved for 2WC model which produced waves smaller than UNC model (the maximum difference was approximately 0.2 m). At the storm peak (at 18:00 UTC on the 28th of January), 2WC model produced an under estimation of  $H_s$ , which balanced the overestimation of the current speed (Fig. 17, left panel). In fact, when coupled in two-way with SWAN, ocean currents were enhanced for the inclusions of wave forces and turbulent kinetic energy injection (Carniel et al., 2009). Despite the mentioned discrepancies, in general, a good agreement between the modeled and observed currents was obtained: in run UNC, the RMSD and Cross-Correlation were 0.04 m/s and 0.70, respectively, whilst when including the effect of waves (run 2WC), the RMSD remained unchanged, whereas the CC increased to 0.75. Additional effect of circulation is the current-induced wave refraction (Fig. 15, right panel). The effect of current was the maximum in the region between Croatian–Istrian Peninsula and the Italian Po river delta, with deviations which reached 20°.

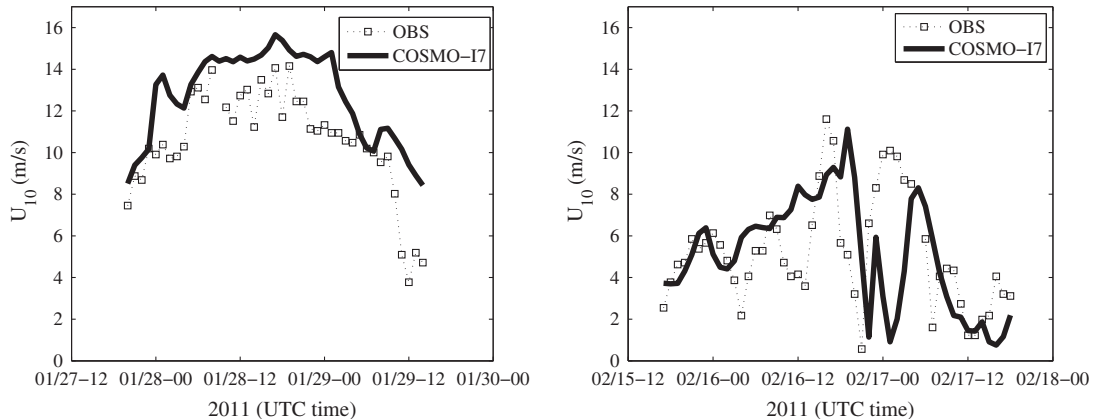


**Fig. 13.** Time series comparison of observed (OBS) and modeled (COSMO-I7) wind speeds at the oceanographic tower *Acqua Alta* for Bora (left panel) and Sirocco (right panel) storms.

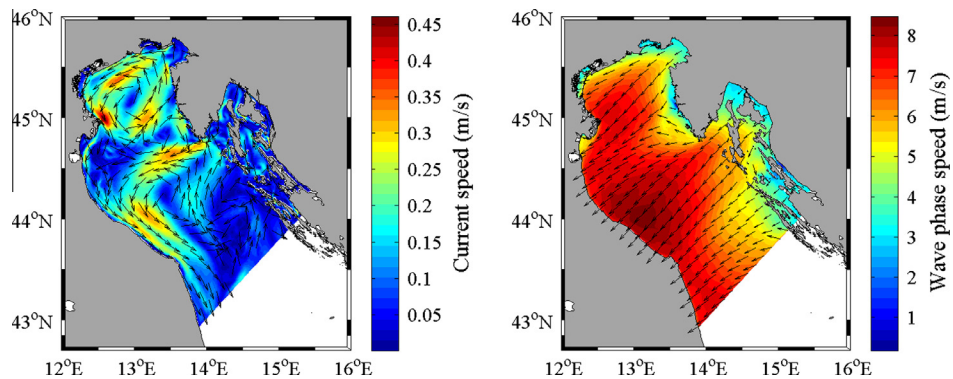


**Fig. 14.** The ROMS-SWAN hindcast results for a Bora event (2011 January, 27 18:00 UTC – 2011 January, 29 12:00 UTC). Storm mean average current (left) and wave phase speed (right) computed in 2WC run. For graphical purposes, current vector arrows are scaled to unity length and decimated by a factor of 25.

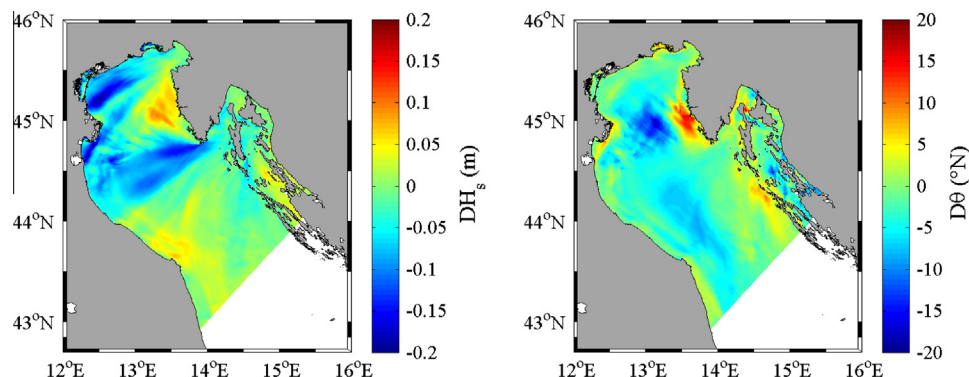


**Fig. 15.** The ROMS-SWAN hindcast results for a Bora event (2011 January, 27 18:00 UTC – 2011 January, 29 12:00 UTC).  $DH_s$  (left panel) and  $D\theta$  (right panel) represent the average difference,  $D$ , of  $H_s$  and mean direction of propagation  $\theta$  between fully coupled (2WC) and uncoupled (UNC) runs.

During the Sirocco storm, wave phase speeds were aligned with along-basin axis and current velocities were limited to 0.1 m/s (Fig. 18). Sirocco current pattern exhibited a single gyre which approached the Croatian coast from South and then followed the Italian coast in a southward direction. Due to small current velocities, waves were slightly sensitive to the ocean currents: maximum differences of  $H_s$  and  $\theta$  between 2WC and UNC runs were limited to 0.1 m and 5°, respectively (Fig. 19). At *Acqua Alta* modeled winds (Fig. 13, right panel) were able to capture the magnitude but not the timing of the first peak. Unfortunately, the second peak was

missed by modeled winds. The first peak shifting and the underestimation in the wind speed after 00:00 UTC (Fig. 13, right panel) on the 17th of February led to an under prediction of the significant wave height peak values for both 2WC and UNC model runs (Fig. 16, right panel). An under prediction was observed on the sea current after 06:00 UTC on the 17th of February (Fig. 17, right panel).

Computed wave and current fields in the Gulf of Venice were also considered for the entire 3-month long simulated period. Mean ocean currents and wave phase speeds during the winter

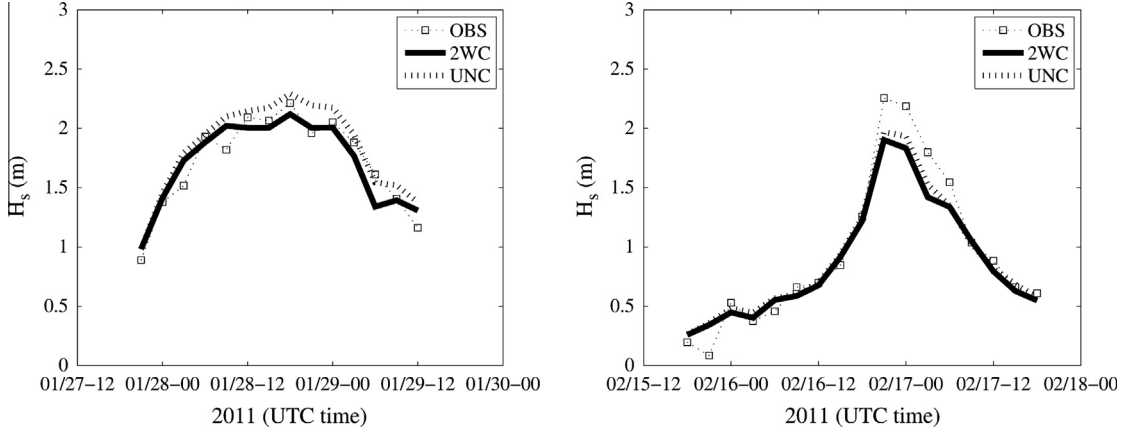


**Fig. 16.** Time series comparison of observed (OBS) and modeled (2WC and UNC) significant wave height  $H_s$  at the oceanographic tower *Acqua Alta*, for the wind events of Bora (left panel) and Sirocco (right panel).

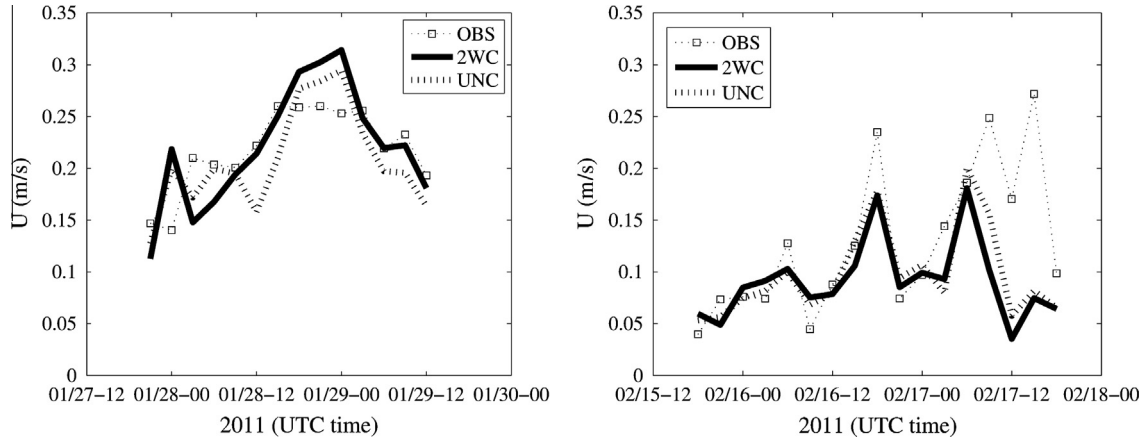


**Fig. 17.** Time series comparison of observed (OBS) and modeled (2WC and UNC) averaged current velocity at the oceanographic tower *Acqua Alta*, for the wind events of Bora (left panel) and Sirocco (right panel).

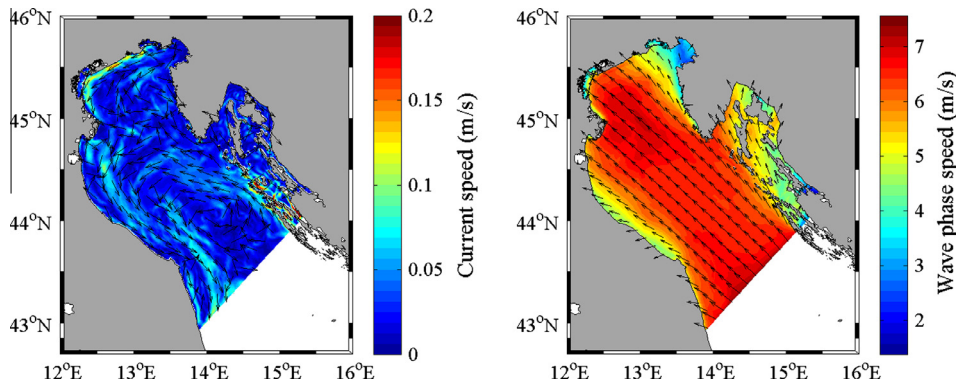


**Fig. 18.** The ROMS-SWAN hindcast results for a Sirocco event (2011 February, 15 18:00 UTC – 2011 February, 17 18:00 UTC). Storm mean average current (left) and wave phase speed (right) computed in 2WC run. For graphical purposes, current vector arrows are scaled to unity length and decimated by a factor of 25.

period bracketing January 1st - March 31st 2011 are shown in Fig. 20. The spatial pattern of mean currents and wave directions highlight that sea circulation and wave propagations were Bora-driven, being waves mostly oriented southwesterly and sea circulation forced to two subgyres. Sirocco contribution is evident close to Croatian coast where along-axis southeastern winds forced currents to be almost parallel to the coast line. For each computational

cell of the fine grid, maximum and minimum differences of  $H_s$  between 2WC and UNC are shown in Fig. 21. In accordance to Bora driven conditions, coupled system produced maximum reduction of  $H_s$  (about 0.6 m) at the center of the northern Adriatic Sea. For the coupled system, increases of  $H_s$  can be observed in Trieste and Kvarner Gulfs, and the Sea area surrounding the Italian Conero promontory (Fig. 21, left panel).

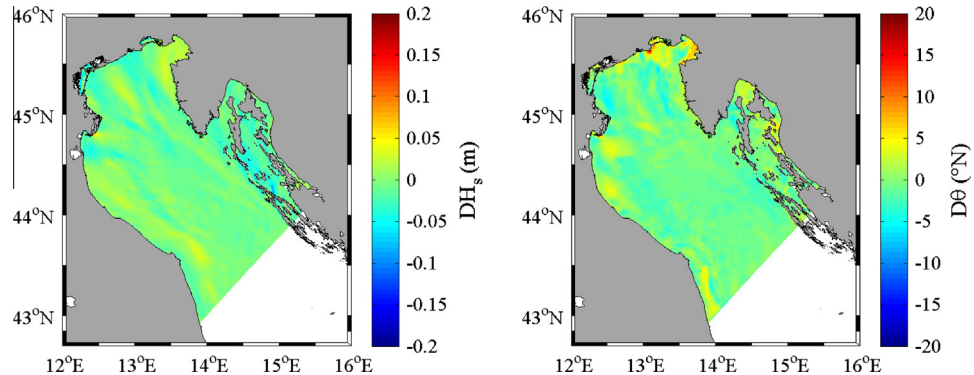


**Fig. 19.** The ROMS–SWAN hindcast results for a Sirocco event (2011 February, 15 18:00 UTC – 2011 February, 17 18:00 UTC).  $DH_s$  (left panel) and  $D\theta$  (right panel) represent the average difference,  $D$ , of  $H_s$  and mean direction of propagation  $\theta$  between fully coupled (2WC) and uncoupled (UNC) runs.

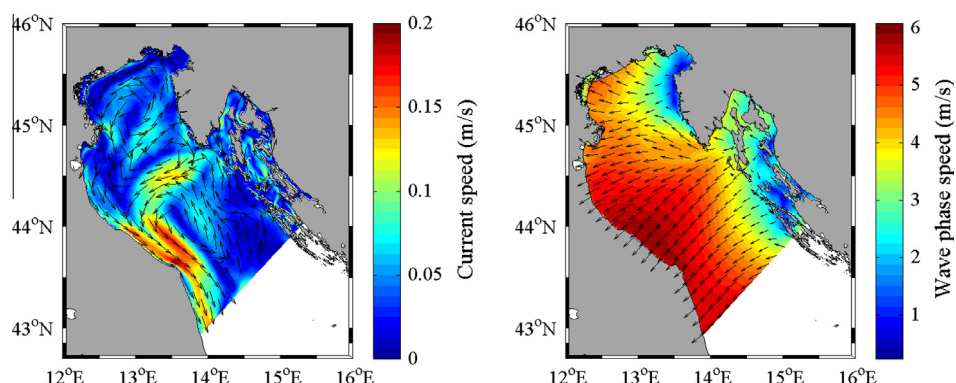


**Fig. 20.** The ROMS–SWAN hindcast results for the whole winter period (January–March 2011). Winter mean average current (left) and wave phase speed (right) computed in 2WC run. For graphical purposes, current vector arrows are scaled to unity length and decimated by a factor of 25.

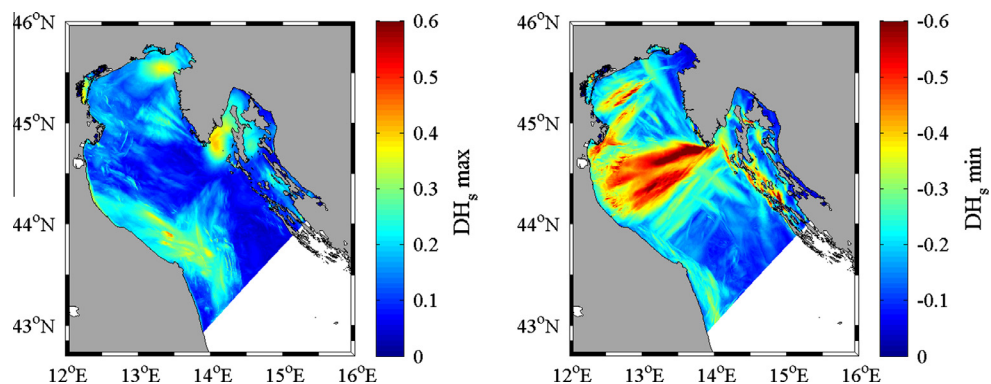


**Fig. 21.** The ROMS–SWAN hindcast results for the whole winter period (January–March 2011). Maximum (left panel) and minimum (right panel)  $DH_s$  of significant wave height between fully coupled (2WC) and uncoupled (UNC) runs.

## 5. Summary and conclusions

It has been shown in previous analysis and studies that ocean current field modifies wave action balance in spectral wave models. Here, the ocean dynamics was investigated using the Coupled Ocean–Atmosphere–Wave–Sediment Transport (COAWST) numerical modeling system (Warner et al., 2010) forced with meteorological forcings provided by high-resolution COSMO-17 model. COAWST is based on ROMS (Regional Ocean Modeling System) and SWAN (Simulating WAves Nearshore) models which are two-way coupled allowing exchange of parameters between ocean and wave models. Wave effects are accounted for through the

inclusion of additional transports of momentum and energy near the sea bed, on the surface, and within the water body (Olabarrieta et al., 2012). In SWAN, current field affects the wave field in two ways: first, the wind input is modified by the current vector; second, the current vector modifies the wave action balance equation. As discussed by Fan et al. (2009b) the effect of current on waves is mostly due to the inclusion of ocean current in the wave action equation, whereas the modification of the forcing term (i.e., the 10-m wind speed) is expected to be more important for wave spectrum tail.

To increase the understanding of ocean–wave interaction in a semi-enclosed basin and its role in storm wind wave predictions,

COAWST was applied within the Adriatic Sea focusing on the northern Adriatic Sea (called Gulf of Venice). Northern Adriatic Sea was used as a representative semi-enclosed basin where significant wave-current interactions could occur. Two computational grids were used: a parent grid with 2-km resolution covered the whole Adriatic Sea, while a child grid, with a resolution of 0.5 km, was implemented in the northern region. This downscaling was necessary in order to reproduce the internal ocean dynamics within the Gulf of Venice, where the ocean circulation is mainly wind-driven and the ROMS-SWAN coupled models were able to capture the wave dynamics in storm conditions. We focused on two storm conditions, as representative of cross-basin and along-basin winds (Bora and Sirocco, respectively).

For model assessment, COAWST and COSMO-I7 outputs were compared to satellite and in situ measurements at *Acqua Alta* tower, 8 miles off the Venice lagoon. With respect to previous studies in the same area (Signell et al., 2005), model validation statistics was improved. Response errors smaller than 10% and 20% for wind magnitude and significant wave height, respectively, clearly indicate a trend of increased quality of atmospheric forcings. This is much more important in an area like the Adriatic Sea where the mountain ridges surrounding the basin induce a topographic effect into the wind field blowing on the water surface.

In the present study, the current sent from the ocean to the wave model was based on the Kirby and Chen (1989) formulation which computes a weighted depth-averaged velocity which accounts for the vertical current structure and the dispersion relation of surface gravity waves. The importance of averaging the vertical currents over a depth controlled by the spectral wave numbers is important in shallow waters, where almost the entire vertical current shear affects wave dynamics. These are the conditions in which the Gulf of Venice is, in fact here the mean water depth is 30 m, and storm conditions produce mean wave length of approximately 40 m.

The main results can be summarized as follows:

1. During a Bora event, in the wave generation channels (e.g., Trieste and Kvarner gulfs) ocean currents produced a reduction of significant wave height. Waves were stretched by the spatially varying current, and wave action  $N$  was modulated in space due to the current advection. A current-induced wave refraction was also observed.
2. Maximum difference of  $H_s$  between coupled and uncoupled runs was found during a Bora event when wave-current interaction on wave action is not negligible, being the  $H_s$  reduction in the order of 0.6 m. Smaller differences were found for the Sirocco storm analyzed.
3. At *Acqua Alta* ROMS-SWAN model hindcast reduced the  $H_s$  during both Bora and Sirocco storms. This was a result of currents propagating in the same directions of waves. The sea current was increased by 0.05–0.10 m/s when models were forced with Bora winds.
4. Results indicate the importance to include ocean circulation effect on waves for hindcast and forecast analysis within a semi-enclosed basin characterized by a wind driven ocean circulation.
5. This study confirmed the capability of COAWST ocean-wave coupled system to simulate ocean and wave dynamics during storm events.

## Acknowledgements

The Authors gratefully acknowledge the funding from the EC FP7/2007–2013 under grant agreement n° 242284 (Project “FIEL-D\_AC”) and from the Italian Ministry of Research FIRB RBFR08D825

grant (Project “DECALOGO”). The authors wish to acknowledge the ARPA-EMR for providing COSMO-I7 meteorological forcings. Luigi “Gigi” Cavaleri is thanked for collecting and organizing satellite data.

## References

- Ardhuin, F., Jenkins, A.D., Belibassakis, K.A., 2008. Comments on “The three-dimensional current and surface wave equations”. *J. Phys. Oceanogr.* 38, 1340–1350.
- Artegiani, A., Bregant, D., Paschini, E., Pinardi, N., Raicich, F., Russo, A., 1997a. The adriatic sea general circulation. 1. Air-Sea interactions and water mass structure. *J. Phys. Oceanogr.* 27, 1492–1514.
- Artegiani, A., Bregant, D., Paschini, E., Pinardi, N., Raicich, F., Russo, A., 1997b. The Adriatic Sea general circulation. 2. Baroclinic circulation structure. *J. Phys. Oceanogr.* 27, 1515–1532.
- Battjes, J.A., Janssen, J.P.F.M., 1978. Energy loss and set-up due to breaking of random waves. In: 16th Int. Conf. Coastal Engineering. ASCE, Hamburg, Germany, pp. 569–587.
- Benetazzo, A., Fedele, F., Carniel, S., Ricchi, A., Buccignani, E., Sclavo, M., 2012. Wave climate of the Adriatic Sea: a future scenario simulation. *Nat. Hazards Earth Syst. Sci.* 12, 2065–2076.
- Bennis, A.C., Arduin, F., Dumas, F., 2011. On the coupling of wave and three-dimensional circulation models: choice of theoretical framework, practical implementation and adiabatic tests. *Ocean Modell.* 40, 260–272.
- Bergamasco, A., Gacic, M., Boscolo, R., Umgieser, G., 1996. Winter oceanographic conditions and water mass balance in the Northern Adriatic (February 1993). *J. Mar. Syst.* 7, 67–94.
- Bergamasco, A., Gačić, M., 1996. Baroclinic response of the Adriatic Sea to an episode of Bora wind. *J. Phys. Oceanogr.* 26, 15.
- Bever, A.J., Harris, C.K., Sherwood, C.R., Signell, R.P., 2009. Deposition and flux of sediment from the Po river, Italy: an idealized and wintertime numerical modeling study. *Mar. Geol.* 260, 69–80.
- Bignami, F., Sciarra, R., Carniel, S., Santoleri, R., 2007. Variability of Adriatic Sea coastal turbid waters from SeaWiFS imagery. *J. Geophys. Res. Oceans* 112, C03S10.
- Bolanos, R., Osuna, P., Wolf, J., Monbaliu, J., Sanchez-Arcilla, A., 2011. Development of the POLCOMS-WAM current-wave model. *Ocean Modell.* 36, 102–115.
- Boldrin, A., Carniel, S., Giani, M., Marin, M., Aubry, F.B., Campanelli, A., Grilli, F., Russo, A., 2009. Effects of Bora wind on physical and biogeochemical properties of stratified waters in the northern Adriatic. *J. Geophys. Res. Oceans* 114, C08S92.
- Booij, N., Ris, R.C., Holthuijsen, L.H., 1999. A third-generation wave model for coastal regions – 1. Model description and validation. *J. Geophys. Res. Oceans* 104, 7649–7666.
- Book, J.W., Perkins, H.T., Cavaleri, L., Doyle, J.D., Pullen, J.D., 2005. ADCP observations of the western Adriatic slope current during winter of 2001. *Prog. Oceanogr.* 66, 270–286.
- Book, J.W., Signell, R.P., Perkins, H., 2007. Measurements of storm and nonstorm circulation in the northern Adriatic: October 2002 through April 2003. *J. Geophys. Res. Oceans* 112.
- Brown, J.M., Bolanos, R., Wolf, J., 2011. Impact assessment of advanced coupling features in a tide-surge-wave model, POLCOMS-WAM, in a shallow water application. *J. Mar. Syst.* 87, 13–24.
- Carniel, S., Warner, J.C., Chiggiato, J., Sclavo, M., 2009. Investigating the impact of surface wave breaking on modeling the trajectories of drifters in the northern Adriatic Sea during a wind-storm event. *Ocean Modell.* 30, 225–239.
- Cavaleri, L., Bergamasco, A., Bertotti, L., Bianco, L., Drago, M., Lovenitti, L., Lavagnini, A., Liberatore, G., Martorelli, S., Mattioli, F., Osborne, A.R., Pedulli, L., Ridolfi, R., Sclavo, M., Serio, M., Tescaro, N., Tibaldi, S., Tosi, E., Vizzoli, D., 1996. Wind and waves in the Northern Adriatic Sea. *Nuovo Cimento Soc. Ital. Fis. C Geophys. Space Phys.* 19, 1–36.
- Cavaleri, L., Bertotti, L., 2003. The characteristics of wind and wave fields modelled with different resolutions. *Q. J. R. Meteorol. Soc.* 129, 1647–1662.
- Cavaleri, L., Bertotti, L., Lionello, P., 1989. Wind-waves evaluation in the Adriatic and Mediterranean Seas. *Int. J. Numer. Methods Eng.* 27, 57–69.
- Cavaleri, L., Sclavo, M., 2006. The calibration of wind and wave model data in the Mediterranean Sea. *Coastal Eng.* 53, 613–627.
- Chapman, D.C., 1985. Numerical treatment of cross-shelf open boundaries in a barotropic coastal ocean model. *J. Phys. Oceanogr.* 15, 1060–1075.
- Charnock, H., 1955. Wind stress on a water surface. *Q. J. R. Meteorol. Soc.* 81, 639–640.
- Cushman-Roisin, B., Gačić, M., Poulaing, P.-M., Artegiani, A., 2001. Physical Oceanography of the Adriatic Sea: Past, Present, and Future. Kluwer Academic Publishers, Dordrecht.
- Durrant, T.H., Greenslade, D.J.M., Simmonds, I., 2009. Validation of Jason-1 and Envisat remotely sensed wave heights. *J. Atmos. Oceanic Technol.* 26, 123–134.
- Dykes, J.D., Wang, D.W., Book, J.W., 2009. An evaluation of a high-resolution operational wave forecasting system in the Adriatic Sea. *J. Mar. Syst.* 78, S255–S271.
- EU, 1999. Ecosystems research Report No. 32. The Adriatic sea, In: Hopkins, T.S., et al. (Ed.), European Commission for Energy, Environment and sustainable development, EUR 18834. FANS project. Supported by EU MAS 3-CT95-003, p. 638.

- Fan, Y., Ginis, I., Hara, T., 2009a. The effect of wind–wave–current interaction on air-sea momentum fluxes and ocean response in tropical cyclones. *J. Phys. Oceanogr.* 39, 1019–1034.
- Fan, Y., Ginis, I., Hara, T., Wright, C.W., Walsh, E.J., 2009b. Numerical simulations and observations of surface wave fields under an extreme tropical cyclone. *J. Phys. Oceanogr.* 39, 2097–2116.
- Flather, R.A., 1976. A tidal model of the northwest European continental shelf. *Mem. Soc. R. Sci. Liege* 10, 141–164.
- Gelci, R., Cazale, H., Vassal, J., 1957. Prévision de la houle. La méthode des densités spectroangulaires. *Bull. Inform. Com. Océanogr. Etude Cotes* 9, 416–435.
- Goring, D.G., Nikora, V.I., 2002. Despiking acoustic Doppler velocimeter data. *J. Hydraul. Eng. ASCE* 128, 117–126.
- Harris, C.K., Sherwood, C.R., Signell, R.P., Bever, A.J., Warner, J.C., 2008. Sediment dispersal in the northwestern Adriatic Sea. *J. Geophys. Res. Oceans* 113.
- Hasselmann, K., 1962. On the non-linear energy transfer in a gravity-wave spectrum Part 1. General theory. *J. Fluid Mech.* 12, 481–500.
- Hasselmann, K., 1988. The WAM model – a third generation ocean wave prediction model. *J. Phys. Oceanogr.* 18, 1775–1810.
- Hasselmann, S., Hasselmann, K., Allender, J.H., Barnett, T.P., 1985. Computations and parameterizations of the nonlinear energy-transfer in a gravity-wave spectrum. Part II: Parameterizations of the nonlinear energy-transfer for application in wave models. *J. Phys. Oceanogr.* 15.
- Hersbach, H., Bidlot, J.-R., 2008. The relevance of ocean surface current in the ECMWF analysis and forecast system. In: Workshop on Ocean–Atmosphere Interactions, Reading, United Kingdom, European Centre for Medium-Range Weather Forecasts, pp. 61–73. [Available online at <<http://www.ecmwf.int/publications/library/do/references/list/28022009>>].
- Janssen, P., 2008. Progress in ocean wave forecasting. *J. Comput. Phys.* 227, 3572–3594.
- Johnsen, H., Kallos, G., Krogstad, H., Athanassoulis, G., Barstow, S., Heiberg, H., Carretero, J.C., Chapron, B., Quefféulou, P., Morales, G., Emmanouil, G., Galanis, G., Gerostathis, T.P., Belibassakis, K.A., Stefanakos, C.N., Croize-Fillon, D., 2005. Development and application of validated geophysical ocean wave products from ENVISAT, ASAR and RA-2 instruments. In: 4th EuroGOOS Conference, Brest, France, June 6–9.
- Kantha, L., Carniel, S., 2003. Comments on “A generic length-scale equation for geophysical turbulence models” by L. Umlauf and H. Burchard. *J. Mar. Res.* 61, 693–702.
- Kara, A.B., Metzger, E.J., Bourassa, M.A., 2007. Ocean current and wave effects on wind stress drag coefficient over the global ocean. *Geophys. Res. Lett.* 34.
- Kirby, J.T., Chen, T.M., 1989. Surface-waves on vertically sheared flows: approximate dispersion relations. *J. Geophys. Res. Oceans* 94, 1013–1027.
- Komen, G.J., Cavalieri, L., Donelan, M., Hasselmann, K., Hasselmann, S., Janssen, P.A.E.M., 1994. Dynamics and Modelling of Ocean Waves. Cambridge University Press.
- Komen, G.J., Hasselmann, S., Hasselmann, K., 1984. On the existence of a fully-developed wind–sea spectrum. *J. Phys. Oceanogr.* 14, 1271–1285.
- Kumar, N., Voulgaris, G., Warner, J.C., 2011. Implementation and modification of a three-dimensional radiation stress formulation for surf zone and rip-current applications. *Coastal Eng.* 58, 1097–1117.
- Kumar, N., Voulgaris, G., Warner, J.C., Olabarrieta, M., 2012. Implementation of the vortex force formalism in the coupled ocean-atmosphere-wave-sediment transport (COAWST) modeling system for inner shelf and surf zone applications. *Ocean Modell.* 47, 65–95.
- Large, W.G., Pond, S., 1981. Open ocean momentum flux measurements in moderate to strong winds. *J. Phys. Oceanogr.* 11, 324–336.
- Lee, C.M., Askari, F., Book, J., Carniel, S., Cushman-Roisin, B., Dorman, C., Doyle, J., Flament, P., Harris, C.K., Jones, B.H., Kuzmic, M., Martin, P., Ogston, A., Orlic, M., Perkins, H., Poulain, P.-M., Pullen, J., Russo, A., Sherwood, C., Signell, R.P., Thaler, D., 2005. Northern Adriatic response to a wintertime Bora wind event. *EOS Trans.* 86, 157–163.
- Longuet-Higgins, M.S., 1970. Longshore currents generated by obliquely incident sea waves. 1. *J. Geophys. Res.* 75, 6778–6789.
- Madsen, O.S., 1994. Spectral wave-current bottom boundary layer flows, Coastal Engineering 1994. In: Proceedings of the 24th International Conference on Coastal Engineering Research Council, Kobe, Japan, pp. 384–398.
- Madsen, O.S., Poon, Y.-K., Gruber, H.C., 1988. Spectral wave attenuation by bottom friction: theory. In: Twenty-first Coastal Engineering Conference, Costa del Sol-Malaga, Spain, June 20–25, pp. 492–504.
- Mason, E., Molemaker, J., Schepetkin, A.F., Colas, F., McWilliams, J.C., Sangra, P., 2010. Procedures for offline grid nesting in regional ocean models. *Ocean Modell.* 35, 1–15.
- Massel, S.R., 1996. Ocean Surface Waves: Their Physics and Prediction. World Scientific Pub. Co. Inc., Singapore – New Jersey – London – Hong Kong.
- McWilliams, J.C., Restrepo, J.M., Lane, E.M., 2004. An asymptotic theory for the interaction of waves and currents in coastal waters. *J. Fluid Mech.* 511, 135–178.
- Mei, C.C., 1989. The Applied Dynamics of Ocean Surface Waves. World Scientific.
- Mellor, G.L., 2008. The depth-dependent current and wave interaction equations: a revision. *J. Phys. Oceanogr.* 38, 2587–2596.
- Michaud, H., Marsaleix, P., Lerédde, Y., Estournel, C., Bourrin, F., Lyard, F., Mayet, C., Arduhin, F., 2011. Three-dimensional modelling of wave-induced current from the surf zone to the inner shelf. *Ocean Sci. Discuss.* 8, 2417–2478.
- Olabarrieta, M., Warner, J.C., Kumar, N., 2011. Wave-current interaction in Willapa Bay. *J. Geophys. Res. Oceans* 116, C12014.
- Olabarrieta, M., Warner, J.C., Armstrong, B., Zambon, J.B., He, R., 2012. Ocean-atmosphere dynamics during Hurricane Ida and Nor’Ida: An application of the coupled ocean-atmosphere-wave-sediment transport (COAWST) modeling system. *Ocean Modell.* 43–44, 112–137.
- Orlanski, I., 1976. Simple boundary-condition for unbounded hyperbolic flows. *J. Comput. Phys.* 21, 251–269.
- Orlic, M., Kuzmic, M., Pasaric, Z., 1994. Response of the Adriatic Sea to the Bora and Sirocco forcing. *Cont. Shelf Res.* 14, 91–116.
- Osuna, P., Monbaliu, J., 2004. Wave-current interaction in the Southern North Sea. *J. Mar. Syst.* 52, 65–87.
- Paklar, G.B., Isakov, V., Koracina, D., Kourafalou, V., Orlic, M., 2001. A case study of Bora-driven flow and density changes on the Adriatic Shelf (January 1987). *Cont. Shelf Res.* 21, 1751–1783.
- Phillips, O.M., 1977. The Dynamics of the Upper Ocean. Cambridge University Press.
- Pierson, W.J., Moskowitz, L., 1964. A proposed spectral form for fully developed wind seas based on the similarity theory of S.A. Kitagorodskii. *J. Geophys. Res.* 69, 5181–5190.
- Pinardi, N., Allen, I., Demirov, E., De Mey, P., Korres, G., Lascaratos, A., Le Traon, P.Y., Maillard, C., Manzella, G., Tziavos, C., 2003. The Mediterranean ocean forecasting system: first phase of implementation (1998–2001). *Annal. Geophys.* 21, 3–20.
- Pullen, J., Doyle, J.D., Hodur, R., Ogston, A., Book, J.W., Perkins, H., Signell, R., 2003. Coupled ocean-atmosphere nested modeling of the Adriatic Sea during winter and spring 2001. *J. Geophys. Res. Oceans* 108.
- Raicich, F., 1994. Note on the flow rates of the Adriatic rivers, Tech. Rep. 561 RF 02/94, CNR Ist. Sper. Tallassogr., Trieste, Italy, 8 pp.
- Roland, A., Cucco, A., Ferrarin, C., Hsu, T.-W., Liu, J.-M., Ou, S.-H., Umgieser, G., Zanke, U., 2009. On the development and verification of a 2-D coupled wave-current model on unstructured meshes. *J. Mar. Syst.* 78, S244–S254.
- Russo, A., Coluccelli, A., Deserti, M., Valentini, A., Benetazzo, A., Carniel, S., 2012. An operational coupled wave-current forecasting system for the northern Adriatic Sea. In: EGU General Assembly Conference Abstracts, Vienna, Austria, 22–27 April, p. 12947.
- Rusu, L., Soares, C.G., 2011. Modelling the wave-current interactions in an offshore basin using the SWAN model. *Ocean Eng.* 38, 63–76.
- Signell, R.P., Carniel, S., Cavalieri, L., Chiggiato, J., Doyle, J.D., Pullen, J., Sclavo, M., 2005. Assessment of wind quality for oceanographic modelling in semi-enclosed basins. *J. Mar. Syst.* 53, 217–233.
- Skamarock, W.C., Klemp, J.B., Dudhia, J., Gill, D.O., Barker, D.M., Wang, W., Powers, J.G., 2005. A Description of the Advanced Research WRF Version 2. NCAR Technical Note, NCAR/TN-468+STR.
- Smolarkiewicz, P.K., 1983. A simple positive definite advection scheme with small implicit diffusion. *Monthly Weather Review* 111.
- Smolarkiewicz, P.K., 1984. A fully multidimensional positive definite advection transport algorithm with small implicit diffusion. *J. Comput. Phys.* 54.
- Soares, C.G., de Pablo, H., 2006. Experimental study of the transformation of wave spectra by a uniform current. *Ocean Eng.* 33, 293–310.
- Stacey, M.W., 1999. Simulation of the wind-forced near-surface circulation in Knight Inlet: a parameterization of the roughness length. *J. Phys. Oceanogr.* 29, 1363–1367.
- Steppeler, J., Doms, G., Schattler, U., Bitzer, H.W., Gassmann, A., Damrath, U., Gregoric, G., 2003. Meso-gamma scale forecasts using the nonhydrostatic model LM. *Meteorol. Atmos. Phys.* 82, 75–96.
- Stewart, R.H., Joy, J.W., 1974. HF radio measurements of surface currents. *Deep Sea Res. Oceanogr. Abstracts* 21, 1039–1049.
- SWAN, 2012. SCIENTIFIC AND TECHNICAL DOCUMENTATION SWAN Cycle III Version 40.81 [Available online at <[http://swanmodel.sourceforge.net/online\\_doc/swanuse/swanuse.html](http://swanmodel.sourceforge.net/online_doc/swanuse/swanuse.html)>].
- Tamura, H., Miyazawa, Y., Oey, L.-Y., 2012. The Stokes drift and wave induced-mass flux in the North Pacific. *J. Geophys. Res.* 117, C08021.
- Tayfun, M.A., Dalrymple, R.A., Yang, C.Y., 1976. Random wave-current interactions in water of varying depth. *Ocean Eng.* 3, 403–420.
- Taylor, K.E., 2001. Summarizing multiple aspects of model performance in a single diagram. *J. Geophys. Res. Atmos.* 106, 7183–7192.
- Uchiyama, Y., McWilliams, J.C., Schepetkin, A.F., 2010. Wave-current interaction in an oceanic circulation model with a vortex-force formalism: Application to the surf zone. *Ocean Modell.* 34, 16–35.
- Umlauf, L., Burchard, H., 2003. A generic length-scale equation for geophysical turbulence models. *J. Mar. Res.* 61, 235–265.
- Warner, J.C., Armstrong, B., He, R.Y., Zambon, J.B., 2010. Development of a coupled ocean-atmosphere-wave-sediment transport (COAWST) modeling system. *Ocean Modell.* 35, 230–244.
- Warner, J.C., Sherwood, C.R., Arango, H.G., Signell, R.P., 2005. Performance of four turbulence closure models implemented using a generic length scale method. *Ocean Modell.* 8, 81–113.
- Warner, J.C., Sherwood, C.R., Signell, R.P., Harris, C.K., Arango, H.G., 2008. Development of a three-dimensional, regional, coupled wave, current, and sediment-transport model. *Comput. Geosci.* 34, 1284–1306.
- Whitham, G.B., 1974. Linear and Nonlinear Waves. Wiley.